PHYSICAL REVIEW A VOLUME 36, NUMBER 9 NOVEMBER 1, 1987

Two-electron excitations in atomic calcium. II. Fine-structure effects

Longhuan Kim and Chris H. Greene
Department of Physics and Astronomy, Louisana State University, Baton Rouge, Louisiana 70803
(Received 12 June 1987)

A simple recoupling frame transformation is shown to adequately describe numerous effects of the spin-orbit interaction which show up in photoionization of the calcium atom. This is accomplished after solving the nonrelativistic Schrödinger equation in LS coupling by an eigenchannel R-matrix method, ignoring all spin-orbit terms in the Hamiltonian. The calculation reproduces most features of the total cross section observed experimentally, and predicts a strong effect of the spin-orbit interaction on partial cross sections, on the photoelectron angular distributions, and on the alignment of the ionic photofragments.

I. INTRODUCTION

A recent R-matrix study of calcium photoionization[1] accounted for the dominant experimental spectral features up to the $Ca^+(4p)$ threshold.[2,3] This work, referred to hereafter as paper I, treated the calcium valence electrons nonrelativistically in LS coupling, ignoring the spin-orbit interaction. In the present paper we show how a geometrical frame transformation allows us to describe an additional class of conspicuous effects generated by this small spin-orbit term in the Hamiltonian. This frame transformation follows in spirit a number of related studies, such as the analysis of fine-structure effects in photodetachment by Rau and Fano,[4] by Lee and Lu,[5] by Lee,[6] and by Taylor and Norcross.[7] The essential physical background is presented by Fano and Rau.[8] In essence, the short-range Hamiltonian will be assumed diagonal in LS coupling owing to dominance of the exchange interaction, whereas the wave function of a photoelectron which escapes to large distances should be characterized in jj coupling since its wavelength depends on the total angular momentum j_i of the residual ionic core.

An eigenchannel R-matrix calculation[1,9–12] provides the required dynamical information in the form of LS-coupled reaction matrices for $^1P^\circ$, $^3P^\circ$, and $^3D^\circ$ symmetries. Using Wigner 9-j coefficients, these LS-coupled reaction matrices are transformed into a 13-channel reaction matrix in a JJ-coupling scheme. Multichannel quantum-defect theory[8,13,14] then predicts observables in the usual fashion, including total and partial photoionization cross sections, photoelectron angular distributions,[15–17] and the alignment[18,19] of the residual ionic fragments.

Inclusion of fine-structure effects causes numerous additional resonances to appear between the $4s$ and $3d$ thresholds which were not present in the LS-coupled photoionization calculation of paper I. For the most part these are weak and narrow, but they show up clearly in Newsom's experimental spectra.[2] Far more dramatic modifications of the calculations in paper I occur close to the spin-orbit-split thresholds $3d_{3/2}$-$3d_{5/2}$ and $4p_{1/2}$-$4p_{3/2}$, where interacting Rydberg series generate an intricate pattern of complicated resonance structures observed by Brown and Ginter.[20] Although the photoelectron asymmetry parameter β and the photoionization-produced ionic alignment $A_0^{\rm col}$ have not been measured for calcium to date, we make predictions of these quantities as well. Not surprisingly, the weak spin-orbit force is seen to affect these anisotropic observables much more strongly than the total cross section. Finally, calculations of the branching ratios show that above the $Ca^+(4p)$ thresholds, photoionization of the calcium ground state predominantly populates the excited $Ca^+(3d)$ levels. This somewhat surprising "population inversion" results more from strong valence electron correlations, however, than from the spin-orbit interaction.

II. METHOD OF CALCULATION

The process we consider in this work is

$$\mathrm{Ca}(J_0)+\gamma(j_\gamma=1)\rightarrow \mathrm{Ca}^+(j_i)+e(l,j) \tag{1}$$

in which photoelectrons are ejected by the electric dipole interaction from a calcium atom in its ground state. This process must satisfy the following set of angular momentum and parity-conservation relations,

$$\mathbf{J}_0+\mathbf{j}_\gamma=\mathbf{j}_i+\mathbf{j}_e=\mathbf{J}\ , \tag{2}$$

$$\pi=\pi_0\pi_\gamma=\pi_i\pi_e\ , \tag{3}$$

where the subscripts 0, γ, i, and e represent the initial atom, the incoming photon, the residual ion, and the photoelectron, respectively.

Our goal is to calculate the cross sections and angular distributions for electrons leaving each accessible ionic state of Ca^+ and also to calculate the alignment of the residual ionic fragment. The calculational procedure can be divided into two separate parts. The first deals with evaluation of the reduced dipole matrix and appropriate dynamical parameters (in the form of a quantum-defect matrix) for all ionization channels involved in the process. The second part calculates the observable quantities using the multichannel quantum-defect theory (MQDT).

For the first part we use the eigenchannel R-matrix method to variationally determine wave functions of the valence electron pair within a volume called the reaction zone having a radius r_0. As in paper I, we use a reaction zone radius $r_0=18$ a.u. throughout. The basis functions used in the variational calculation are Slater-determinantal two-electron wave functions coupled to form a definite orbital and spin angular momentum. They are constructed from one-electron independent-particle wave functions after solving the radial Schrödinger equation for an electron moving in the Hartree-Slater potential field of Ca^{2+} (including a polarization correction). Outside the reaction zone, where the potential is Coulombic, the wave function of the outermost electron is represented by a linear combination of regular and irregular Coulomb functions in each channel. These wave functions are matched at the boundary of the reaction zone to determine the relevant short-range MQDT parameters. Detailed accounts of the theoretical basis for this type of calculation can be found in the previous paper (I) and other papers.[1,9–12]

To include the effects of fine structure, a frame transformation from LS to JJ coupling is required. For each ionization threshold $Ca^+(n_i l_i)$ with $l_i>0$, instead of one resonance series expected from an LS-coupling calculation, there are at least two separate resonance series with slightly different phases and energy intervals due to the energy splitting of the threshold. These two thresholds have two different values of the total angular momentum, $j_i=l_i\pm\frac{1}{2}$. In this work the energy splitting of these thresholds is taken from experimental data instead of calculating it by including the spin-orbit interaction term explicitly in the Hamiltonian. To calculate the photoelectron asymmetry parameter and the ionic fragment alignment we have utilized the angular momentum transfer method developed by Dill, Fano, and others.[15–18]

A. Frame transformation

The reduced dipole matrix and the quantum-defect matrix defined in Eq. (26) of paper I are first calculated as functions of energy in LS coupling, and the corresponding matrices in the JJ-coupling scheme are obtained by a frame transformation,[4–8]

$$\underline{\mu}^{JJ}=\underline{V}\,\underline{\mu}^{LS}\underline{V}^{T}\ , \tag{4}$$

where $\underline{V}$ is the usual transformation matrix involving a Wigner 9-J coefficient

$$\begin{aligned}V_{JJ,LS}&=\langle (s_i l_i)j_i,(sl)j \mid (s_i s)S,(l_i l)L\rangle\\&=[(2j_i+1)(2j+1)(2S+1)(2L+1)]^{1/2}\\&\quad\times\begin{Bmatrix}s_i & l_i & j_i\\ s & l & j\\ S & L & J\end{Bmatrix}\ .\end{aligned} \tag{6}$$

Here subscript i refers to the valence electron of the residual Ca^+ ion, while lower case angular momenta having no subscripts (s,l,j) refer to the photoelectron. Here we consider photoionization of the calcium ground state, which leads to a $J=1$ final continuum state. The 13 fragmentation channels involved in the LS-coupling calculations are

$$4s\varepsilon p\ {}^1P^\circ,\ 3d\varepsilon p\ {}^1P^\circ,\ 3d\varepsilon f\ {}^1P^\circ,\ 4p\varepsilon s\ {}^1P^\circ,\ 4p\varepsilon d\ {}^1P^\circ,\ 4s\varepsilon p\ {}^3P^\circ,\ 3d\varepsilon p\ {}^3P^\circ,$$
$$3d\varepsilon f\ {}^3P^\circ,\ 4p\varepsilon s\ {}^3P^\circ,\ 4p\varepsilon d\ {}^3P^\circ,\ 3d\varepsilon p\ {}^3D^\circ,\ 3d\varepsilon f\ {}^3D^\circ,\ 4p\varepsilon d\ {}^3D^\circ\ .$$

The final JJ coupling fragmentation channels are

$$4s_{1/2}\varepsilon p_{1/2},\ 4s_{1/2}\varepsilon p_{3/2},\ 3d_{3/2}\varepsilon p_{1/2},\ 3d_{3/2}\varepsilon p_{3/2},\ 3d_{5/2}\varepsilon p_{3/2},\ 3d_{3/2}\varepsilon f_{5/2},\ 3d_{5/2}\varepsilon f_{5/2},$$
$$3d_{5/2}\varepsilon f_{7/2},\ 4p_{1/2}\varepsilon s_{1/2},\ 4p_{3/2}\varepsilon s_{1/2},\ 4p_{1/2}\varepsilon d_{3/2},\ 4p_{3/2}\varepsilon d_{3/2},\ 4p_{3/2}\varepsilon d_{5/2}\ .$$

In Table I we give the calculated ${}^3P^\circ$ and ${}^3D^\circ$ quantum-defect matrices at the $3d$ and $4p$ thresholds. With this table and Table III of paper I, it should be possible to reproduce most of our results in the energy range considered.

B. Photoelectron angular distribution

The angular distribution of the photoelectron is characterized by an asymmetry parameter β. For a given ionic state i of the target atom the relevant asymmetry parameter β_i is a function of the incident photon energy. Taking the direction of linear polarization of the incident photon to define the z axis, we have for each ionic state a differential cross section

$$\frac{d\sigma_i}{d\Omega}=\frac{\sigma_i}{4\pi}[1+\beta_i P_2(\cos\theta)]\ , \tag{7}$$

where σ_i is the partial photoionization cross section in channel i, integrated over Ω.

One basic difficulty faced by most approaches treating an anisotropy produced by photoionization is the great multiplicity of degenerate continuum channels contributing coherently to the anisotropy. In earlier work, Dill and Fano[15–17] introduced a new set of continuum chan-

TABLE I. Quantum-defect matrices μ_{ij}.

	$4s\varepsilon p$	$3d\varepsilon p$	$3d\varepsilon f$	$4p\varepsilon s$	$4p\varepsilon d$
		(a) At the $Ca^+(3d)$ threshold			
$^3P^\circ$	−0.0495	0.0388	0.0094	−0.0751	0.0710
	0.0388	−0.1280	−0.0316	−0.1999	−0.1140
	0.0094	−0.0316	−0.0732	−0.0452	0.2157
	−0.0751	−0.1999	−0.0452	0.3834	0.0505
	0.0710	−0.1140	0.2157	0.0505	−0.1379
$^3D^\circ$	$3d\varepsilon p$	$3d\varepsilon f$	$4p\varepsilon d$		
	0.1618	0.0265	0.1267		
	0.0265	−0.0102	0.1311		
	0.1267	0.1311	−0.0081		
		(b) At the $Ca^+(4p)$ threshold			
$^3P^\circ$	−0.0917	0.0407	−0.0081	−0.0967	0.0704
	0.0407	−0.2063	−0.0224	−0.1629	−0.0980
	−0.0081	−0.0224	−0.0487	−0.0425	0.1408
	−0.0967	−0.1629	−0.0425	0.3681	0.0497
	0.0704	−0.0980	0.1408	0.0497	−0.0804
$^3D^\circ$	−0.2184	0.0139	0.1017		
	0.0139	−0.0103	0.1064		
	0.1017	0.1064	−0.0288		

nels whose contributions to β add incoherently. These channels are characterized not by the usual JJ-coupling scheme but rather by j_t, the angular momentum transferred between unobserved photofragments,

$$\mathbf{j}_t=\mathbf{j}_i+\mathbf{s}-\mathbf{J}_0=\mathbf{j}_\gamma-\mathbf{l}\ . \tag{8}$$

Here $\mathbf{s}$ and $\mathbf{l}$ are the spin and orbital angular momenta of the photoelectron. $\mathbf{j}_\gamma$ is the unit angular momentum transferred to the target by the electric dipole photon, and $\mathbf{j}_i$ is the angular momentum of the ionic state after the photoionization. Using this set of continuum channels, the expression for β takes the simple form of an incoherent average over j_t,[15–17]

$$\beta_i=\sum_{j_t}\sigma(j_t)\beta(j_t)\Big/\sum_{j_t}\sigma(j_t)\ , \tag{9}$$

where $\sigma(j_t)$ is the partial cross section for photoionization into the continuum channel characterized by the angular momentum transfer quantum number j_t. For each given j_t there are either two contributing values of the photoelectron orbital angular momentum $l=j_t\pm1$ (parity favored) and or else a single partial wave $l=j_t$ (parity unfavored). For parity-unfavored angular momentum transfers $\beta(j_t)$ is simply equal to -1. For the parity-favored transfer $\beta(j_t)$ is expressed as

$$\beta(j_t)=\frac{(j_t+2)|\bar S_+|^2+(j_t-1)|\bar S_-|^2-6[j_t(j_t+1)]^{1/2}\mathrm{Re}(\bar S_+\bar S_-^*)}{(2j_t+1)[|\bar S_+|^2+|\bar S_-|^2]}\ . \tag{10}$$

The partial cross sections associated with each j_t are

$$\sigma_{\mathrm{fav}}(j_t)=\frac{\lambda}{4\pi}[(2j_t+1)/(2J_0+1)]\times[|\bar S_+(j_t)|^2+|\bar S_-(j_t)|^2] \tag{11}$$

for parity-favored transfers, and

$$\sigma_{\mathrm{unf}}(j_t)=\frac{\lambda}{4\pi}[(2j_t+1)/(2J_0+1)]|\bar S_0(j_t)|^2 \tag{12}$$

for parity-unfavored transfers. In Eqs. 10–12, $\bar S_\pm(j_t)\equiv\bar S(j_t,l=j_t\pm1)$ and $\bar S_0(j_t)\equiv\bar S(j_t,l=j_t)$, where $\bar S(j_t,l)$ denotes the photoionization amplitude for a given j_t and l. The relation between $\bar S(j_t,l)$ and the reduced dipole-matrix element connecting the ground state to the incoming-wave-normalized final state is given in Ref. 17.

C. Alignment of the residual Ca^+ fragment

If the incident photons are linearly polarized and the direction of the escaping photoelectron is not observed, then the polarization and angular distribution of the ionic fluorescence excited by the photoionization are completely specified in terms of the Fano-Macek alignment parameter[19]

$$A_0^{\mathrm{col}}(j_i)=\left\langle j_i\left|\frac{3j_{iz}^2-\mathbf{j}_i^2}{\mathbf{j}_i^2}\right|j_i\right\rangle\ , \tag{13}$$

where j_{iz} is the z component of the total ionic angular momentum operator $\mathbf{j}_i$. For linearly polarized incident

photons the polarization axis defines the z axis, while for unpolarized incident photons the z axis is the photon propagation axis. Alternatively, if the state emits no dipole radiation [as is true of $Ca^+(3d)$], then its alignment can be measured using laser-induced fluorescence.[21]

Introducing **t**, the angular momentum transferred to the photoelectron, $A_0^{\rm col}(j_i)$ can also be represented as an incoherent average over a set of universal alignment functions for each j_i and t, weighted by corresponding transition probabilities,

$$A_0^{\rm col}(j_i)=\frac{\sum_t |S(j_i;t)|^2 A_0^{\rm col}(j_i;t)}{\sum_t |S(j_i;t)|^2} . \tag{14}$$

Unlike $\beta(j_t)$ in Eq. (10), $A_0^{\rm col}(j_i;t)$ is a purely geometrical quantity, containing no dynamical information. It is a universal function[18] of j_i and t with three possible values $t=j_i\pm1$ and $t=j_i$. For linearly polarized incident light it is just

$$A_0^{\rm col}(j_i;t)=\begin{cases} -\frac{2}{5}+\frac{3}{5(j_i+1)}, & t=j_i+1 \text{ (parity favored)} \\ -\frac{2}{5}-\frac{3}{5j_i}, & t=j_i-1 \text{ (parity favored)} \\ \frac{4}{5}-\frac{3}{5j_i(j_i+1)}, & t=j_i \text{ (parity unfavored)} \end{cases} \tag{15}$$

while for unpolarized incident light the right-hand side of Eq. (15) must be multiplied by $-\frac{1}{2}$.

As we see from Eq. (14), the alignment $A_0^{\rm col}(j_i)$ is an incoherent average over the three branches of the universal alignment function $A_0^{\rm col}(j_i;t)$, weighted by the dynamical quantity $|S(j_i;t)|^2$. The expression relating these amplitudes $S(j_i;t)$ to the incoming-wave dipole-matrix elements is given by Eq. (13) of Ref. 18. (That equation contains a misprint which can be corrected by changing the factor $(2t+1)^{1/2}/3^{1/2}$ on the right-hand side into the factor $(-1)^{J+J_0}[(2t+1)(2J+1)]^{1/2}$.) For all nontrivial cases with $j_i>\frac{1}{2}$, $A_0^{\rm col}(j_i;t)$ is negative for parity-favored angular momentum transfers and positive for parity-unfavored transfers. For $j_i\le\frac{1}{2}$, $A_0^{\rm col}(j_i;t)=0$. Note that unless the parity-unfavored transfer dominates in a specific process the alignment function $A_0^{\rm col}(j_i)$ usually has negative values, as expected classically.[18]

III. RESULTS

We have obtained predictions for σ_i, β_i, and $A_0^{\rm col}(j_i)$ as functions of energy for the $4s$, $3d$, and $4p$ ionic states. The total cross section σ is obtained by summing the cross sections σ_i over all open ionic channels. The energy range considered in this work is from just above the $4s$ threshold up to just above the $4p_{3/2}$ threshold. The number of energetically accessible ionic states of Ca^+ increases with energy, of course. Here we treat three energy ranges in detail, namely, between the $4s$ and $3d$ thresholds, between the $3d$ and $4p$ thresholds, and between the two $4p$ thresholds ($4p_{1/2}$ and $4p_{3/2}$). The dipole velocity formula was used for all calculations in this paper.

The energy difference between the two $3d$ thresholds ($3d_{3/2}$ and $3d_{5/2}$) is very small (about 0.0002 a.u.) making it extremely difficult experimentally to separate the photoelectrons escaping from the two ionic states. Accordingly, the β parameters for the $3d$ state are obtained as a weighted average over the $3d_{3/2}$ and $3d_{5/2}$ states while the cross section for $3d$ is the sum of the cross section for $3d_{3/2}$ and $3d_{5/2}$.

A. Photoionization spectra

In Fig. 1 we show the calcium photoionization spectrum for photon wavelengths between 1650 and 1920 Å. Figure 1(a) is Newsom's experimental result.[2] Figure 1(b) is our calculated result. The experimental ground-state energy has been used to convert the final-state energy into a photon wavelength scale. Figure 1(c) shows the β parameter to be discussed later. The normalization of Newsom's experimental cross section has been re-

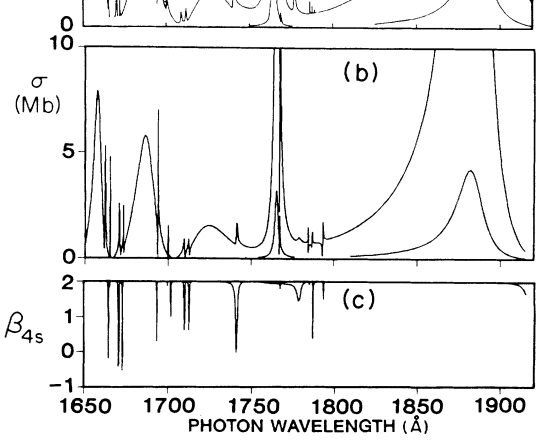

FIG. 1. Cross section for photoionization of the calcium atom for incident photon wavelengths between 1650 and 1920 Å; (a) experiment of Newsom (Ref. 2); (b) calculated spectrum; (c) asymmetry parameter characterizing the photoelectron angular distribution. Insets in (a) and (b) show the cross section reduced by a factor of 10.

vised (as in paper I) according to the newer absolute measurement of McIlrath and Sandeman[22] at 1887.5 Å. The global features of our calculated spectrum in this energy range have been discussed in paper I where results were obtained in LS coupling for the $^1P^\circ$ final state, ignoring all fine-structure effects. The results were in generally good agreement with experiment except for those small resonances introduced by the spin-orbit interaction, which mixes the $^1P^\circ$, $^3P^\circ$, and $^3D^\circ$ LS-coupled states. These small resonances are reproduced faithfully in our present result giving even better agreement with most fine experimental details. There are still some discrepancies. The small resonance at 1777 Å is apparently too small in our calculation. Also, the three resonances near 1790 Å are much farther apart from each other than are the experimental resonances. The amplitude of the very narrow resonances between the main $3dnp$ resonances are also somewhat different from the experiment, but we have not attempted to give a quantitative estimate of these discrepancies.

Figure 2 shows the spectrum for energies between the $3d$ and $4p$ thresholds. The measurement of Connerade *et al.*[3] is not absolute, which is the reason we have not labeled the experimental ordinate in Fig. 2(a). The agreement between the experiment and our calculation in this energy range is poorer than at lower energies, but it still improves on previous calculations, including the LS-coupling results of paper I.

Figure 3 compares the photoionization spectrum between the two $4p$ thresholds ($4p_{1/2}$ and $4p_{3/2}$) with the experimental results of Brown and Ginter.[20] In their paper the photoabsorption spectrum is given as a densitometer tracing without absolute scale. To compare roughly with our calculation, we have converted it into a photoionization spectrum by inverting it and renormalizing the overall magnitude to give optimum agreement. The spectrum in this energy range is a simple periodic

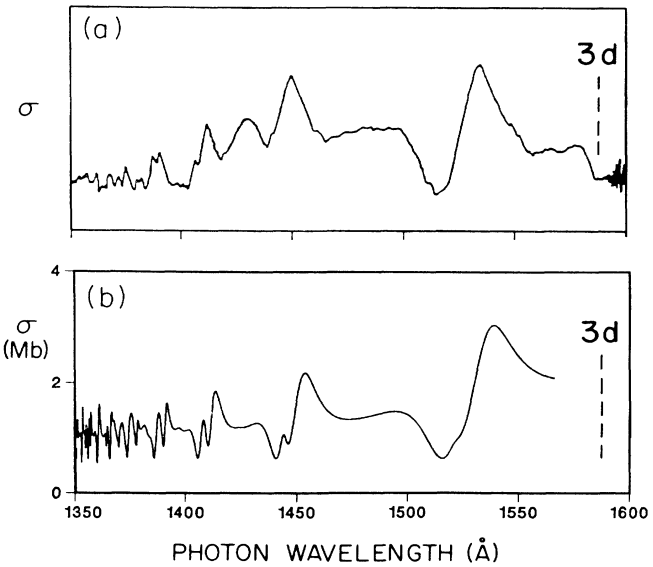

FIG. 2. Total photoionization cross section of calcium for incident photon wavelength between 1350 and 1600 Å; (a) experiment of Connerade *et al.* (Ref. 3); (b) calculated spectrum.

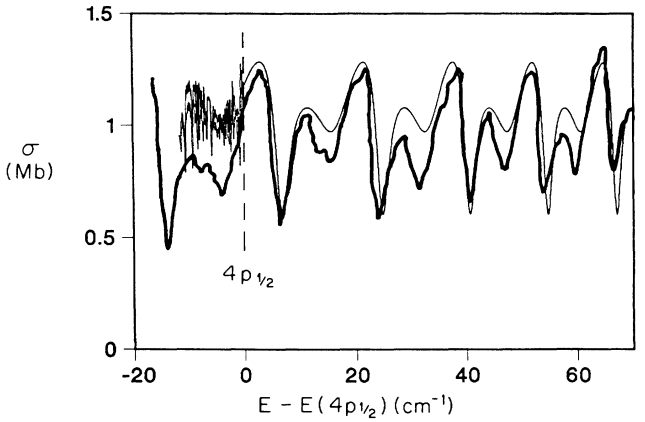

FIG. 3. Calcium photoionization cross section between the $4p_{1/2}$ and $4p_{3/2}$ thresholds as a function of the total energy (relative to the $4p_{1/2}$ threshold energy) compared with experimental results of Brown and Ginter (Ref. 20). The thick line is the experimental curve, while the thin line is our calculated result.

pattern, similar to that documented thoroughly for the rare-gas atoms.[23] Only the first several resonances are shown in the figure. The rest of the spectrum up to the $4p_{3/2}$ threshold simply repeats the pattern with increasing frequency. Below the $4p_{1/2}$ threshold the experimental resolution cannot resolve the series of narrow resonances having extremely high principal quantum numbers ($n > 95$ in the range shown in Fig. 3). These high $4p_{1/2}ns$ and $4p_{1/2}nd$ resonances induce rapid oscillations in the cross section whose average value joins smoothly to the continuum cross section just above $Ca^+(4p_{1/2})$. (We have not attempted to included enough energy points in our theoretical curve to represent the fine features just below the $4p_{1/2}$ threshold accurately.)

B. Photoelectron angular distribution

We show calculated asymmetry parameters of electrons ejected by photoionization of calcium in its ground state in Figs. 4–6. In each energy range, the β parameters oscillate regularly, in phase with the oscillatory variations of the cross section. The fine structure plays a small role when the energy is far below any given threshold. With increasing energy not only the number of res-

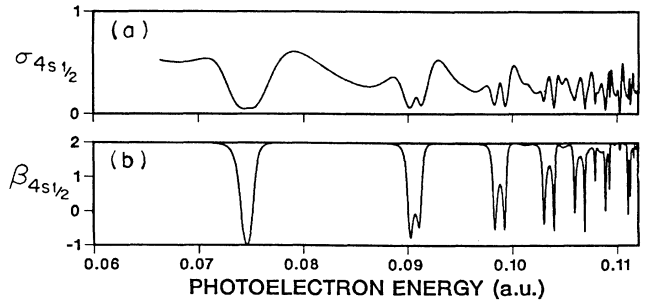

FIG. 4. Partial photoionization cross sections (in units of Mb) and the photoelectron asymmetry parameter for the $4s_{1/2}$ residual ionic state, at energies between the $3d$ and $4p$ thresholds.

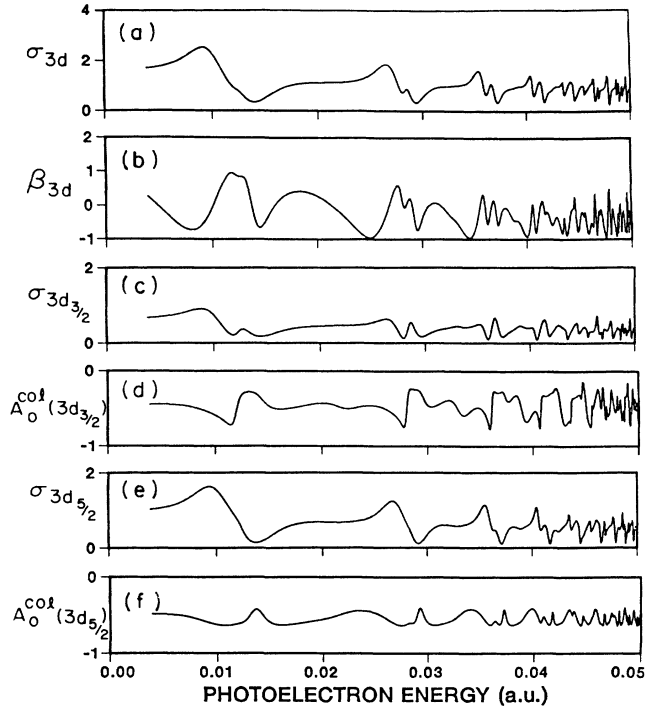

FIG. 5. Partial photoionization cross section (a) and average asymmetry parameter (b) for the $3d$ ionic states at energies between the $3d$ and $4p$ thresholds. Partial photoionization cross section (c) and alignment function (d) for the $3d_{3/2}$ ionic state; (e) and (f) are the same as (c) and (d) but for the $3d_{5/2}$ ionic state.

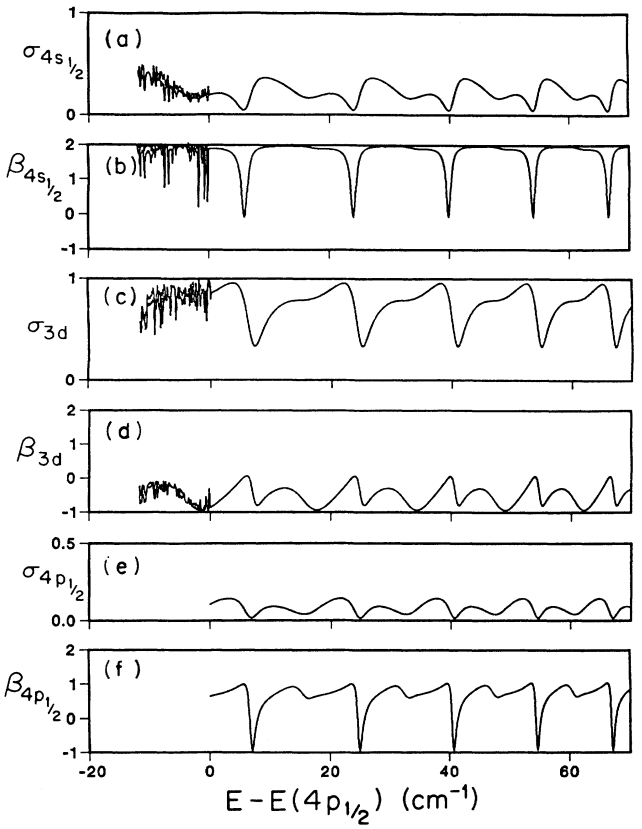

FIG. 6. Partial photoionization cross sections and asymmetry parameters for total energies between the $4p_{1/2}$ and $4p_{3/2}$ thresholds. (a) and (b) refer to the $4s_{1/2}$ ionic state, (c) and (d) refer to the $3d$ ionic state, and (e) and (f) refer to the $4p_{1/2}$ ionic state.

onances in a given energy interval increases but also the shape of the higher-lying resonances changes as the effective quantum number ν_i in the spin-orbit-split channels begins to differ appreciably. Profiles of the β parameters are determined by Eqs. (9)–(12) and by the fact that $\beta_{\rm unf}=-1$. In Eq. (10) only the third term can contribute negative values to β. It is obvious that if β_i is negative it is due to either the coherent term involving $\bar{S}_+\bar{S}^*_-$ in Eq. (10) and/or from the parity-unfavored angular momentum transfers.

1. β_{4s}

In this case the orbital angular momentum quantum number l has only one value $l=1$. The angular momentum transfer is simply the total spin S of the valence electron pair and can be either 0 (parity favored) or 1 (parity unfavored). This leads to [see Eq. (11)] $\beta_{\rm fav}=2$ and $\beta_{\rm unf}=-1$. In the absence of any spin-orbit interaction β would always be exactly 2 in this case. The parity-unfavored terms are present only because of the spin-orbit interaction, which is most important close to a fine-structure-split pair of thresholds. The resulting β_{4s} is shown as a function of the energy in Fig. 1(c), Fig. 4, and Fig. 6(b). Over most of the spectrum β_{4s} is equal to 2 except near fine-structure resonances. In our calculation the fine-structure effects are included only through their modification of the Ca^+ thresholds which affect just the imposition of large-r boundary conditions using MQDT. If we exclude the fine-structure effect by artificially forcing all spin-orbit-split thresholds to be degenerate, we find the constant value $\beta_{4s}=2$ independently of the energy.

2. β_{3d}

We show in Fig. 5(b) and Fig. 6(d) the average value of the asymmetry parameter which would be measured if these two photoelectron groups are not resolved,

$$\beta_{3d}=\frac{(\sigma_{3d_{3/2}}\beta_{3d_{3/2}}+\sigma_{3d_{5/2}}\beta_{3d_{5/2}})}{(\sigma_{3d_{3/2}}+\sigma_{3d_{5/2}})}\ . \tag{16}$$

We see that there are resonances, both in the cross section and in the angular distribution asymmetry parameter. Over most of the spectrum β_{3d} has negative values. This does not derive from the parity-unfavored terms, unlike the negative values of β_{4s} close to resonances. Eliminating the energy splitting of the $3d_{3/2}$ and $3d_{5/2}$ thresholds in the quantum-defect calculation changes little of the overall shape of β_{3d} in this energy range because the weight of the parity-unfavored channel is generally much smaller than that of the parity-favored

channels. The generally negative values of β_{3d} are thus somewhat unusual, and are seen to derive from the interference of the S_+ and S_- amplitudes in Eq. (10). The sign of this interference term is determined by their relative phase, which involves a complicated combination of several reduced dipole amplitudes. Near each autoionizing resonance the resonant variation of the continuum phases and amplitudes causes both the cross section and the β parameter to oscillate with energy. While it is difficult to give much further interpretation to these variations, we can state definitively that the generally negative values of β_{3d} are a consequence of the specific nature of the correlations between the valence electrons, and *not* produced mainly by the spin-orbit interaction.

3. $\beta_{4p_{1/2}}$

Figure 6(f) shows the integrated cross section σ and the β parameter for the $4p_{1/2}$ ionic state at energies between the $4p_{1/2}$ and $4p_{3/2}$ thresholds. The pattern of $\beta_{4p_{1/2}}$ is similar to β_{4s} [Fig. 6(b)] except that the "base" value for the $\beta_{4p_{1/2}}$ is much lower than 2. Another difference is that there are additional resonances between the major resonance series while β_{4s} has nearly flat value between the resonances. Since only $l=2$ and $l=0$ are allowed and j_t must equal 1, there is no parity-unfavored term.

C. Alignment parameters

The alignment parameters $A_0^{\rm col}(3d_{3/2})$ and $A_0^{\rm col}(3d_{5/2})$ are shown as functions of the photoelectron energy in Fig. 5(d) and 5(f) (for energies between the $3d$ and $4p$ thresholds) and in Fig. 7 (for energies above the $4p_{1/2}$ threshold). The photoionization cross sections related to each ionic state are shown along with the $A_0^{\rm col}(j_i)$ curves. Note that $A_0^{\rm col}(4s)=A_0^{\rm col}(4p_{1/2})=0$, whereby only the alignment of the two $3d$ ionic states needs to be discussed. Compared to the asymmetry parameter β, the alignment parameters have less fluctuation as the energy crosses autoionizing resonances. The average value is roughly -0.6 for both $3d_{3/2}$ and $3d_{5/2}$. The fluctuation of $A_0^{\rm col}(3d_{5/2})$ is smaller than that of $A_0^{\rm col}(3d_{3/2})$, as can be understood from Eq. (15). Neglecting the parity-unfavored term, the alignment is expected to lie between the two parity-favored branches of the universal alignment function. For $j_i=\frac{3}{2}$ it ranges from -0.8 to -0.16 while for $j_i=\frac{5}{2}$ it ranges from -0.64 to -0.229. Since $A_0^{\rm col}(j_i;t)$ does not depend on energy, the energy dependence of $A_0^{\rm col}(j_i)$ is determined by only the two independent ratios of the three squared amplitudes $|S(j_i;t)|^2$. As the energy approaches the $4p_{1/2}$ threshold the role of the parity-unfavored term becomes increasingly important, resulting in a more complicated energy dependence.

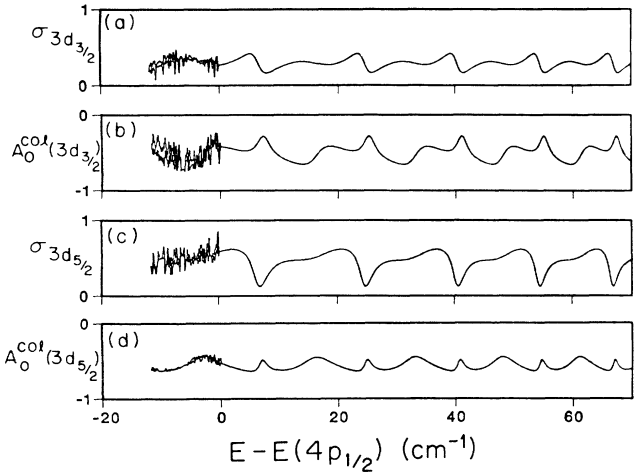

FIG. 7. Partial photoionization cross sections and alignment parameters for total energies between the $4p_{1/2}$ and $4p_{3/2}$ thresholds. (a) and (b) refer to the $3d_{3/2}$ ionic state, and (c) and (d) refer to the $3d_{5/2}$ ionic state.

D. Above the $4p_{3/2}$ threshold

Above the $4p_{3/2}$ threshold the parity-unfavored term vanishes and the asymmetry parameter and the alignment function become slowly varying, nearly constant quantities. We do not present results for energies much higher than threshold as we are uncertain about how rapidly our present calculation deteriorates at energies above the $4p_{3/2}$ threshold. In any case, our predictions for the β parameters and alignment parameters at an energy just above the $4p_{3/2}$ threshold are given in Table II.

It is also evident both from Table II and from the figures that the dominant partial cross sections are the ones producing $Ca^+(3d)$ levels. The same conclusion was reached in the *LS*-coupling calculation of Scott *et al.*[24] This implies a severe breakdown of the independent-electron model for calcium in this energy range, which would predict that only the ground state of Ca^+ is populated by the photoionization process. Of course it is by now clear that the independent-electron model has little validity for two-electron systems at low energies. Still, it is interesting that photoionization of atomic calcium produces such a strong population inversion. In particular the metastable levels $Ca^+(3d_{3/2})$ and $Ca^+(3d_{5/2})$ are seen in Table II to produce 64% of the photoionization processes at this energy. This inversion

TABLE II. Calculated values of σ_i, β_i, and $A_0^{\rm col}(j_i)$ at the $4p_{3/2}$ threshold.

	$4s$	$3d_{3/2}$	$3d_{5/2}$	$4p_{1/2}$	$4p_{3/2}$
σ_i (Mb)	0.1787	0.2669	0.4003	0.0652	0.1304
β_i	2.000	−0.6374	−0.6370	0.6873	0.5323
$A_0^{\rm col}(j_i)$	0.0	−0.5159	−0.5896	0.0	−0.5913

has essentially nothing to do with the spin-orbit interaction, deriving instead from the strong electron correlations which dominate the spectrum of calcium.

Note added in proof. A very similar treatment of fine-structure effects on Sr photoabsorption has recently been completed by M. Aymar, J. Phys. B (to be published), giving excellent results.

ACKNOWLEDGMENTS

This work was supported in part by the National Science Foundation. One of us (C.H.G.) also received partial support from the Alfred P. Sloan Foundation.

[1]Chris H. Greene and Longhuan Kim, Phys. Rev. A **36**, 2706 (1987).
[2]G. H. Newsom, Proc. Phys. Soc. London **87**, 975 (1966).
[3]J. P. Connerade, M. A. Baig, W. R. S. Garton, and G. H. Newsom, Proc. R. Soc. London, Ser. A **371**, 295 (1980).
[4]A. R. P. Rau and U. Fano, Phys. Rev. A **4**, 1751 (1971).
[5]C. M. Lee and K. T. Lu, Phys. Rev. A **8**, 1241 (1973).
[6]C. M. Lee, Phys. Rev. A **11**, 1692 (1975).
[7]K. T. Taylor and D. Norcross, Phys. Rev. A **34**, 3878 (1986).
[8]U. Fano and A. R. P. Rau, *Atomic Collisions and Spectra* (Academic, Orlando, 1986).
[9]C. H. Greene, Phys. Rev. A **28**, 2209 (1983); **32**, 1880 (1985).
[10]H. Le Rouzo and G. Raseev, Phys. Rev. A **29**, 1214 (1984).
[11]P. F. O'Mahony and C. H. Greene, Phys. Rev. A **31**, 250 (1985); P. F. O'Mahony, Phys. Rev. A **32**, 908 (1985).
[12]M. Aymar, E. Luc-Koenig, and S. Watanabe, J. Phys. B (to be published).
[13]M. J. Seaton, Rep. Prog. Phys. **46**, 97 (1983).
[14]C. H. Greene and Ch. Jungen, Adv. At. Mol. Phys. **21**, 51 (1985).
[15]Dan Dill and U. Fano, Phys. Rev. Lett. **29**, 1203 (1972).
[16]U. Fano and Dan Dill, Phys. Rev. A **6**, 185 (1972).
[17]Dan Dill, Phys. Rev. A **7**, 1976 (1973).
[18]Chris H. Greene and Richard N. Zare, Phys. Rev. A **25**, 2031 (1982).
[19]U. Fano and J. H. Macek, Rev. Mod. Phys. **45**, 553 (1973).
[20]C. M. Brown and M. L. Ginter, J. Opt. Soc. Am. **70**, 87 (1980).
[21]C. H. Greene and Richard N. Zare, J. Chem. Phys. **78**, 6741 (1983).
[22]T. J. McIlrath and R. J. Sandeman, J. Phys. B **5**, L217 (1972).
[23]W. R. Johnson, K. T. Cheng, K.-N. Huang, and M. Le Dourneuf, Phys. Rev. A **22**, 989 (1981).
[24]P. Scott, A. E. Kingston, and A. Hibbert, J. Phys. B **16**, 3945 (1983).